TEM studies of Pt-Al-Cr-Ru Alloys

by M.B. Shongwe*†, M.J. Witcomb†, L.A. Cornish*†, and M.J. Papo†‡

Transaction Paper

Synopsis

Pt-based alloys are being developed for high-temperature applications with the aim of replacing some of the currently used Ni-based superalloys (NBSAs) in the highest temperature applications. The Pt-based alloys have a similar structure to the NBSAs, and since Pt is more chemically inert than nickel and has a higher melting point, they can potentially be used at higher temperatures, up to 1 300°C, and in more aggressive environments. Several experimental Pt-based alloys were studied at Mintek, and an optimum composition was found to be Pt_{84}:Al_{11}:Ru_2:Cr_3 (at.%). On the basis of hardness and microstructure, a later study identified a new optimum: Pt_{78}:Al_{11}:Ru_5:Cr_6 (at.%). There are at least two Pt_3Al allotropes, and the high-temperature cubic structure has better properties than the lower temperature tetragonal form, and so needs to be stabilized.

This work describes the latest results obtained in transmission electron microscopy (TEM) studies of the quaternary Pt-based superalloys. These results are both interesting and important, because the samples have a higher precipitate density compared to those from earlier work. The precipitate morphology is mainly cubic, with minor areas having irregular-shaped precipitates. The high volume fraction of the precipitates is a major breakthrough, since the objective of this work is to improve the alloys. A prior disadvantage was that the proportion of the precipitates was too low in samples before this work, especially compared with the work from Germany on Pt-Al-Cr-Ni-based alloys as well as the NBSAs.

TEM ~Pt_3Al diffraction patterns were studied, and for each diffraction pattern, many possible lattice point combinations were tried, with the angle between the lattice spots as well as interplanar spacings being calculated for each phase (cubic or tetragonal) to match the measured results. An overall analysis of the diffraction results indicates that the cubic phase fitted the experimental lattice points with much lower errors compared to the tetragonal phase. Thus, with the close match achieved with the cubic structure, the structure of ~Pt_3Al precipitates is likely to be cubic.

X-ray diffraction has been carried out on selected samples, and the results confirmed the presence of cubic ~Pt_3Al and (Pt). Different X-ray diffractometers were used to further verify the results, and the results were also compared with those from TEM.

Keywords
Platinum alloys, TEM, precipitation strengthening.

Introduction

The temperature constraints of existing materials restrict the performance of turbine engines used in aviation and power generation. The Ni-based superalloys (NBSAs) that are currently used in these demanding applications are already operating at up to 90 per cent of their melting temperature. Any further significant improvements in the operating temperatures will require the development of a new generation of materials, with higher melting points[1]. One approach is to develop alloys with microstructures analogous to the γ/γ′ structures of NBSAs, but based on elements with higher melting points. In such a microstructure, the face-centred cubic (fcc) matrix is strengthened by coherent precipitates of an intermetallic compound with the $L1_2$ (ordered, fcc) crystal structure. The fcc platinum-group metals Pt, Ir, and Rh are candidates for such an alloy development programme because of their high melting points and exceptional environmental resistance[2]. There is one important difference between the NBSAs and the platinum-based alloys. There is only one form of Ni_3Al, whereas the phase Pt_3Al has at least two forms[3], and the more desirable high temperature cubic $L1_2$ form needs to be stabilized. There is one, if not two, lower temperature forms. One is the distorted $L1_2$ structure $D0'_C$, which originates from a martensitic-type transformation at ~400°C[4]. A low temperature modified $D0'_C$ structure has also been identified[5].

A research programme at Mintek and the University of the Witwatersrand, together with other institutions, is focused on developing Pt-based ultra-high-temperature alloys, exploiting platinum's high melting point, fcc crystal structure, and superior environmental resistance[6,7]. Hill *et al.*[7] selected ternary Pt-X-Z compositions to yield two-phase microstructures consisting of the fcc (Pt) matrix

* *School of Chemical and Metallurgical Engineering, University of the Witwatersrand.*

† *DST/NRF Centre of Excellence in Strong Materials, hosted by the University of the Witwatersrand.*

† *Advanced Materials Division, Mintek.*

 SA ISSN 2225-6253. This paper was first presented at the ZrTa2011 New Metals Development Network Conference, 12–14 October 2011, Mount Grace Country House & Spa, Magaliesburg.

and ordered fcc ($L1_2$) Pt_3X precipitates. Two-phase microstructures, leading to strengthening, were achieved in the Pt-Ti-Z and Pt-Al-Z systems[8]. Alloys in these systems showed promising mechanical properties at room temperature, with hardness values higher than 400 HV_{10} and high resistance to crack initiation and propagation. The alloys containing Al exhibited considerably better oxidation behaviour than the other alloys, and this was attributed to the formation of a protective alumina scale. Internal oxidation was observed in alloys containing Ti instead of Al, and this was presumed to be the cause of their inferior properties. Al was considered as the essential addition in order to develop an oxidation-resistant alloy[8], therefore further work was focused on Pt-Al-Z alloys only.

The effects of some ternary alloying additions (Ti, Cr, Ru Ta, and Ir) on the precipitate morphology, lattice mismatch, and properties of two-phase (Pt)/~Pt_3Al alloys were investigated by Hill *et al.*[9]. The crystal structure and morphology of the ~Pt_3Al phase were examined, and the compressive strengths and melting temperatures of the alloys were also determined. It was found that Ti, Cr, and Ta partitioned to ~Pt_3Al and stabilized the $L1_2$ form of this phase. The ~Pt_3Al phase in these alloys had cuboid morphologies and a small lattice misfit with the matrix (about 0.7 per cent). The tetragonal $D0'_C$ form of ~Pt_3Al was observed in the alloys containing Ru and Ir. The ~Pt_3Al in these alloys formed in groups shaped like a Maltese cross, which may have resulted from the higher lattice misfit in these alloys (-1 to -1.2 per cent) for the $D0'_C$ crystal structure of the ~Pt_3Al[9].

Investigation of displacive transformations in platinum alloys, using optical microscopy, scanning electron microscopy with energy dispersive spectrometry (SEM-EDS), X-ray diffraction (XRD), and thermal analysis have been carried out by Biggs *et al.*[10,11]. A series of Pt-Al-Ru alloys in the platinum-rich end of the ternary phase diagram were selected for study. For platinum contents at around 73 at.% or above, the low-temperature $D0'_C$ Pt_3Al structure and (Pt) were observed[11]. Alloys containing less than 73 at.% Pt consisted of a two-phase mixture of the cubic Pt_3Al and a platinum-rich solid solution. The ruthenium-rich solid solution (Ru) contained at least 20 at.% Pt, but negligible aluminium. The tetragonal Pt_3Al phase, which forms by a displacive transformation, was found to be highly twinned. XRD suggested that the phase was cubic Pt_3Al. However, in view of the microstructural observation, according to Biggs *et al.*[11] the Pt_3Al phase was tetragonal.

In a study by Douglas *et al.*[5] on the microstructure of binary and ternary Pt alloys, the Pt_3Al precipitates had a trimodal size distribution, ranging from less than 50 nm to greater than 1 µm. The larger precipitates were found to consist of stacked plates that are twin-related, and each twin plate contained a high density of thin platelets lying perpendicular to the *c*-direction. Electron diffraction experiments showed an unexpected result in the form of extra spots in the diffraction pattern. These extra spots, as well as the appearance of high-resolution TEM lattice images, could be fully explained by two modifications of the $D0'_c$ unit cell: one that was 1.5 times the length of the *c*-axis of this unit cell, and one that was 0.5 times the length of the unit cell. The *c*-axis of the unit cell of the precipitate was aligned along the *a*- and *b*-axes of the matrix unit cell. This matrix/precipitate orientation relationship formed in order to relieve the lattice misfit[5].

The best ternary alloys were Pt-Al-Cr and Pt-Al-Ru, and a quaternary was targeted from a combination of these alloys[12,13]. Experimentation gave Pt_{84}:Al_{11}:Ru_2:Cr_3 (at.%) as the best composition with a reasonable proportion of precipitates and good properties, including a HV_{10} of 472±14, although the precipitate volume fraction was only about 30 per cent. Heat treatments were undertaken to increase the precipitate volume fraction[13–17]. More recently[18–20], a series of different Pt-Al-Cr-Ru alloys was studied to improve the precipitate volume fraction, especially after ranges of hardnesses were found for the same alloy compositions. Another research direction is the attempt at partially substituting for the expensive and highly dense platinum with an element that also increases the melting point of (Pt), the platinum solid solution. The candidates here are niobium[21–25] and vanadium[26].

Niobium (Nb) is a possible addition to increase the alloy's melting point[23–25], but only binary phase diagram data are available. Although work has been done on the Pt-Al-Nb ternary system, there were initially no reported data for the Pt-Cr-Nb system. As-cast samples of the Pt-Cr-Nb system have been investigated using scanning electron microscopy with energy-dispersive X-ray spectroscopy (SEM-EDX) and XRD[23,24]. The results have been used to plot a solidification projection, and all binary phases have been found to extend into the ternary, with (Cr) having the least extension of ~2 at.%. The (Pt), ~$NbCr_2$, (Nb), ~Nb_3Pt, ~$NbPt_2$ phases extend around 20 at.% into the ternary[23,24]. Odera *et al.*[26] are currently studying the addition of V to the Pt-Al-Cr-Ru system, which can possibly act as a solid solution strengthener, and perhaps increase the alloy's melting temperature[3]. There were no reported data for Pt-Cr-V, and a study of the system will give an indication of the optimum V content in the Pt-based alloys.

Experimental procedure

Sample preparation for TEM

Arc melted buttons of a nominal weight[20] 3.5 g were heat treated in air in a Lenton muffle furnace at 1 500°C for 18 hours, followed by a quench in water; then annealing at 1 100°C for 120 hours and air cooling. A section of about 250 µm in thickness was cut from the centre of the button. A cylindrical disc of about 3 mm in diameter was cut from the cores of the 250 µm thick plates using a Gatan 601 ultrasonic disc cutter. The discs were thermally bonded to a small glass plate using a 130°C melting wax and inserted into a steel holder and mechanically ground on a 15 mm diamond polishing disc to a thickness of about 90 µm. The surfaces of the samples were polished using 6 µm and 3 µm diamond paste followed by a 0.025 µm alumina suspension. Final thinning of samples was carried out in a Gatan 691 Precision Ion Polishing System (PIPS) using argon gas. Ion milling was done at 5 keV for 3 hours at an angle of 5°, and then at 4.5° for perforation. Subsequently, a final milling was carried out at 2.5 keV at 4.5° for about 4 minutes to reduce the amount of ion damage.

Samples were viewed using a Philips CM200 transmission electron microscope at 197 keV. However, it was not possible

to resolve the details of the microstructure due to ion damage that had fully covered the surface of the sample. To remove the ion damage, samples were electropolished using a method developed by Witcomb[27]. The samples were immersed in a solution made up of equal amounts of phosphoric, nitric, and sulphuric acids at 2.8 VAC. The temperature was maintained at 20°C and the sample was positioned between two Pt electrodes. The cleaning time was about 30 seconds. After cleaning, the structure of ~Pt_3Al precipitates in a (Pt) matrix could be clearly seen. Prior to insertion in the microscope, the microscope holder containing the sample was cleaned in a Gatan plasma cleaner for 30 minutes to remove surface carbon contamination. Electron diffraction patterns were taken in a microdiffraction mode using a small electron probe size, typically in the nanometer range.

Measurements of electron diffraction patterns

A crystalline specimen will diffract the electron beam strongly through well-defined directions (measured as angles, θ) dependent on electron wavelength and crystal lattice spacing according to Bragg's law[28]. The spots in the diffraction pattern correspond to the reciprocal lattice of the investigated crystal. It is possible to determine the crystallographic orientation and type of material by the measurements of the spacing between spots and angles between the vectors[28–30].

Figure 1 shows a simplified schematic diagram illustrating how measurements were done on the diffraction patterns to determine the spacing between the spots and interplanar angles. The transparent diffraction pattern micrograph was placed on a light box to make the lattice spots clearer. The angles (θ_A, θ_B, and θ_C) were measured using a protractor. The total distance for lattice spots intersected by an angle line was measured using a 'travelling microscope', and the distance between the lattice spots was found by dividing the total distance by the total number of points intersected.

X-ray diffraction was also carried out on the Pt-Al-Cr-Ru samples to determine if the ~Pt_3Al phase was tetragonal or cubic, and the lattice parameters were obtained for both tetragonal and cubic structures. Since the camera constant (λL) of the microscope had been measured using a polycrystalline aluminium sample and employing Equation [1], the distance R between two defined spots on the diffraction pattern was calculated using Equations [1] to [3]. The interplanar angles were calculated using Equations [4] and [5][29–31].

$$R = \frac{\lambda L}{d} \qquad [1]$$

where R is the radius of a given $h\ k\ l$ ring (or spot spacing for single crystal), d is the interplanar spacing for the $h\ k\ l$ plane, λ is the wavelength of the electrons, and L, the camera length, is the effective distance between the sample and the recording device.

$$\text{Cubic crystal} \quad d_{hkl} = \frac{a}{\sqrt{h^2 + k^2 + l^2}} \qquad [2]$$

$$\text{Tetragonal crystal:} \quad d_{hkl} = \frac{ac}{\sqrt{\left(h^2 + k^2\right)c^2 + l^2 a^2}} \qquad [3]$$

The interplanar angle ϕ between the plane $(h_1k_1l_1)$, of spacing d_1, and the plane $(h_2k_2l_2)$, of spacing d_2, may be found from the following equations.

Cubic crystal:

$$\cos\phi = \frac{h_1h_2 + k_1k_2 + l_1l_2}{\sqrt{\left(h_1^{\,2} + k_1^{\,2} + l_1^{\,2}\right)\left(h_2^{\,2} + k_2^{\,2} + l_2^{\,2}\right)}} \qquad [4]$$

Tetragonal crystal:

$$\cos\phi = \frac{\dfrac{h_1h_2 + k_1k_2}{a^2} + \dfrac{l_1l_2}{c^2}}{\sqrt{\left(\dfrac{h_1^{\,2} + k_1^{\,2}}{a^2} + \dfrac{l_1^{\,2}}{c^2}\right)\left(\dfrac{h_2^{\,2} + k_2^{\,2}}{a^2} + \dfrac{l_2^{\,2}}{c^2}\right)}} \qquad [5]$$

The calculated distance (R) between the lattice spots and angles were compared with the measured distance and angles in order to deduce whether the ~Pt_3Al phase was cubic or tetragonal.

Results

The XRD results confirmed the presence of ~ Pt_3Al. Tetragonal and cubic Pt_3Al were matched against the experimental XRD pattern and were found to fit the pattern with the exception of a few peaks that could not be matched. The unmatched peaks were matched against the XRD pattern of the plasticine in the sample holder; however, two peaks for the tetragonal phase and two for peaks the cubic phase still remained unmatched, and these are thought to be due to noise disturbances during measurements. The lattice parameters deduced from the XRD results were a = 3.7084 Å (cubic) and a = 5.4398 Å, b = 8.0247 Å (tetragonal). These values were used to calculate the possible interplanar angles and the interplanar spacings, thus spot spacing for the TEM diffraction patterns.

Figure 2 shows a typical TEM microstructure for nominal Pt_{82}:Al_{12}:Ru_2:Cr_4 (at.%) with ~Pt_3Al precipitates in a (Pt) matrix. There was a great improvement in the proportion of ~Pt_3Al precipitates, which were the highest seen to date in a Pt-based alloy. The precipitates varied in size, but were around 200 nm. Diffraction patterns of the ~Pt_3Al phase were

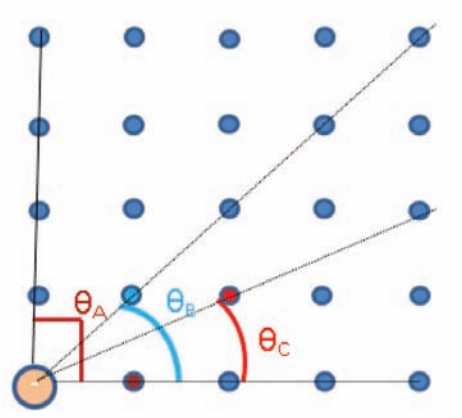

Figure 1—Simplified schematic diagram of a diffraction pattern illustrating measurements of spacing between spots and interplanar angles

TEM studies of Pt-Al-Cr-Ru Alloys

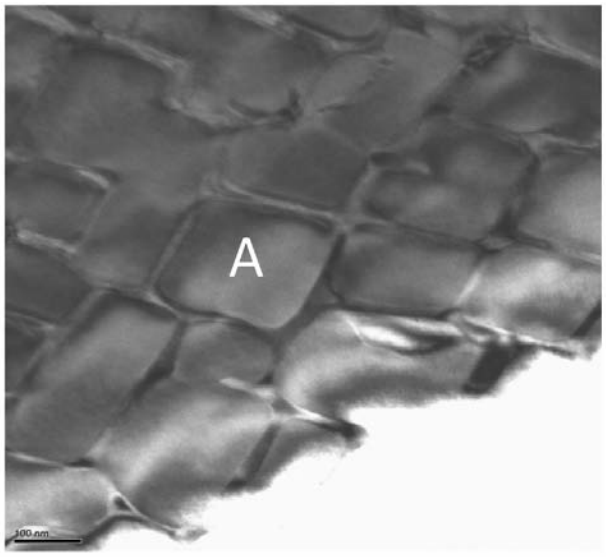

Figure 2—TEM micrograph for nominal Pt_{82}:Al_{12}:Ru_2:Cr_4, showing ~Pt_3Al precipitates, an example is marked A, in a (Pt) matrix

taken from precipitates such as 'A' in Figure 2 by tilting to a different zone axis and employing precipitates from a number of different regions.

For each diffraction pattern, many combinations of *h k l* values were possible for different diffraction spot spacings and angles between different lattice planes. Tables I to V show summaries of the calculated results and the error between the measured and calculated results for both cubic and tetragonal structures. Figures 3 to 6, show different zone axis diffraction patterns obtained for the ~Pt_3Al precipitate from TEM with the possible lattice *h k l* combinations to match the measured distances between spots and angles between planes.

Figure 3(b) shows the best fit with Figure 3(a) for the cubic ~Pt_3Al structure, the zone axis being [1 1 0]. In contrast, Figure 3(c) shows the best fit with Figure 3(a) for the tetragonal ~Pt_3Al structure, the zone axis being [0 1 0]. Tables I and II shows the measured and calculated values for the different spot spacings and interplanar angles for the cubic and tetragonal structures respectively. While the spot spacings for the cubic structure show a larger error than the tetragonal structure, the reverse is the case for the interplanar angles.

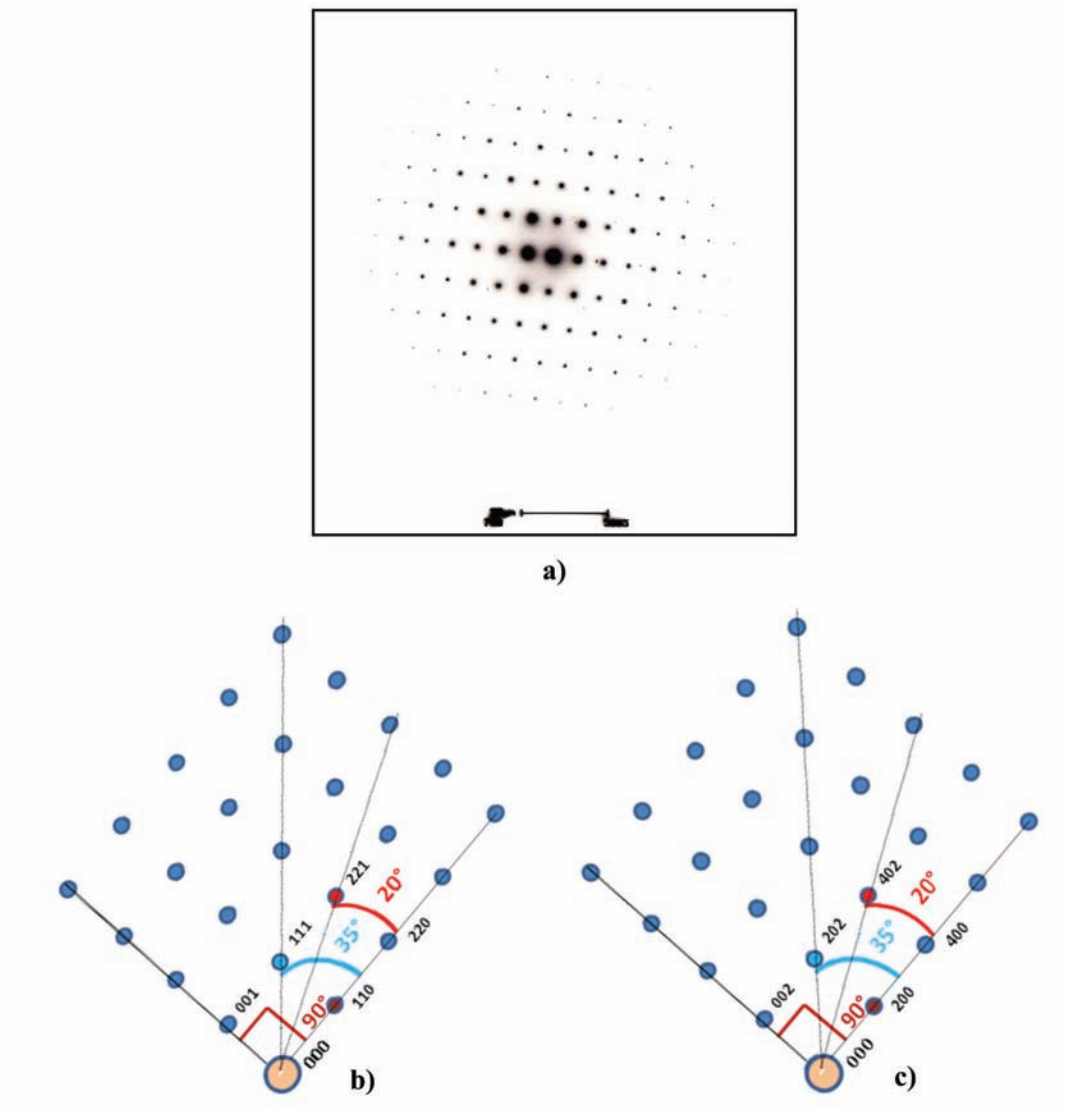

Figure 3. (a) TEM diffraction pattern for a ~Pt_3Al precipitate in a nominal Pt_{78}:Al_{11}:Ru_5:Cr_6 (at.%) alloy. (b) and (c) show schematic diagrams of a different reciprocal lattice points system and measured angles corresponding to the cubic [1 1 0] and tetragonal [0 1 0] zone axis respectively

Table I

Summary of the best possible fit of lattice points and comparison of calculated and measured results for cubic Pt_3Al for Figure 3 (b)

			Spacing			Angles			
Lattice point			Measured	Calculated	Error	Interplanar	Measured	Calculated	Error
h	*k*	*l*	(Å)	(Å)	(%)	angles	(°)	(°)	(%)
1	1	0	5.85	6.25	6.4	-	-	-	-
0	0	1	4.16	4.42	5.9	θ_A 001 110	90	90	0
1	1	1	7.18	7.66	6.3	θ_B 111 110	35	35.26	0.7
2	2	1	12.45	13.27	6.2	θ_C 221 110	20	19.47	2.7

Table II

Summary of the best possible fit of lattice points and comparison of calculated and measured results for tetragonal Pt_3Al for Figure 3 (c)

			Spacing			Angles			
Lattice point			Measured	Calculated	Error	Interplanar	Measured	Calculated	Error
h	*k*	*l*	(Å)	(Å)	(%)	angles	(°)	(°)	(%)
2	0	0	5.85	6.03	3.0	-	-	-	-
0	0	2	4.16	4.09	1.7	θ_A 002 200	90	90	0
2	0	2	7.18	7.28	1.4	θ_B 202 200	35	34.12	2.5
4	0	2	12.45	12.73	2.2	θ_C 402 200	20	18.72	6.8

This could mean that the particular precipitate was tetragonal, and according to Biggs *et al.*[31] this might be expected if the composition of the alloy is within 74.6–76.6 at.% Pt. However, since the cubic phase had a close match to the diffraction pattern (Table I), more zone axes were needed to assess the structure of the ~Pt_3Al phase.

For the diffraction pattern shown in Figure 4(a), a possible combination of lattice points is shown in Figure 4(b) for the cubic ~Pt_3Al structure. No near combination could be found for the tetragonal structure. Table III displays the measured and calculated values for the different spot spacings and interplanar angles for the cubic structure.

Figure 5(b) shows the best fit with Figure 5(a) for the cubic ~Pt_3Al structure, the zone axis being [0 0 1]. No near fit could be found for the tetragonal structure. Table IV lists the measured and calculated values for the different spot spacings and interplanar angles for the cubic structure.

Figure 6(b) shows the best identified combination of lattice points to fit the diffraction pattern in Figure 6(a) for the cubic ~Pt_3Al structure with the zone axis [0 2 1]. Table V lists the measured and calculated values for the different spot spacings and interplanar angles for the cubic structure.

Discussion

The ~Pt_3Al precipitates in the quaternary Pt-based analogue of NBSAs have a uniform size distribution. The precipitate volume fraction is higher than that obtained by Hüller *et al.*[32]

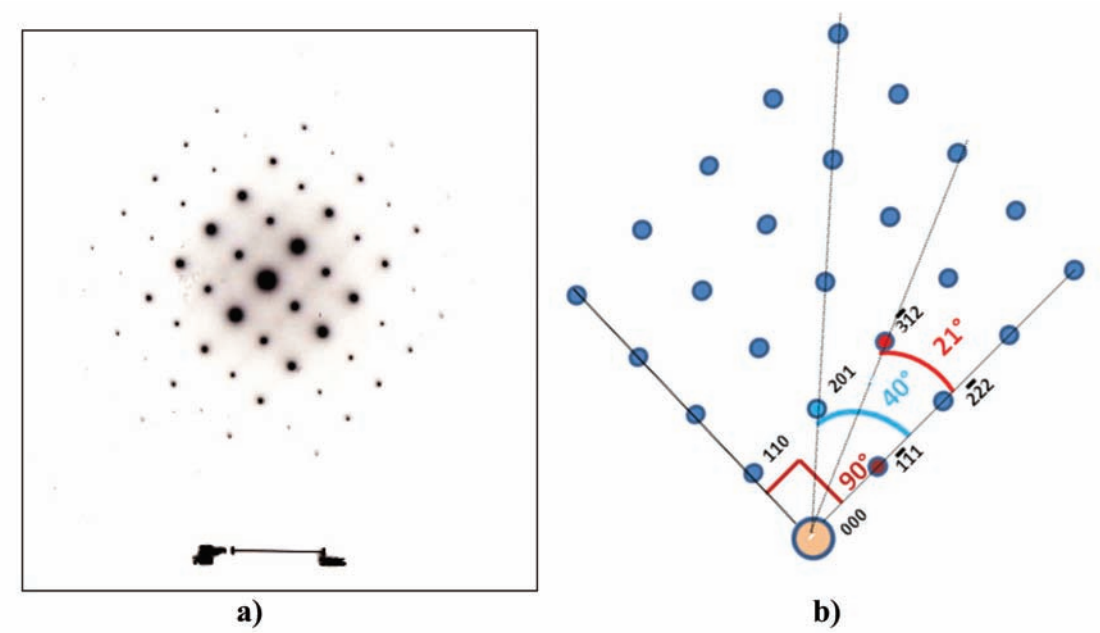

Figure 4—(a) TEM diffraction pattern for a ~Pt3Al precipitates in a nominal Pt_{78}:Al_{11}:Ru_5:Cr_6 (at.%) alloys, (b) schematic diagram of the reciprocal lattice points system and measured angles corresponding to the cubic [1 1 2] zones axis.

Table III

Summary of the best possible fit of lattice points and comparison of calculated and measured results for cubic Pt_3Al for Figure 4 (b)

			Spacing			Angles			
Lattice point			Measured	Calculated	Error	Interplanar	Measured	Calculated	Error
h	*k*	*l*	(Å)	(Å)	(%)	angles	(°)	(°)	(%)
1	1	1	7.13	7.66	6.9	-	-	-	-
1	1	0	5.85	6.25	6.4	θ_A 110 1 1	90	90	0
2	0	1	9.23	9.89	6.7	θ_B 201 1 1	40	39.23	2.0
3	1	2	15.04	16.55	9.1	θ_C 3 2 1 1	21	22.21	5.8

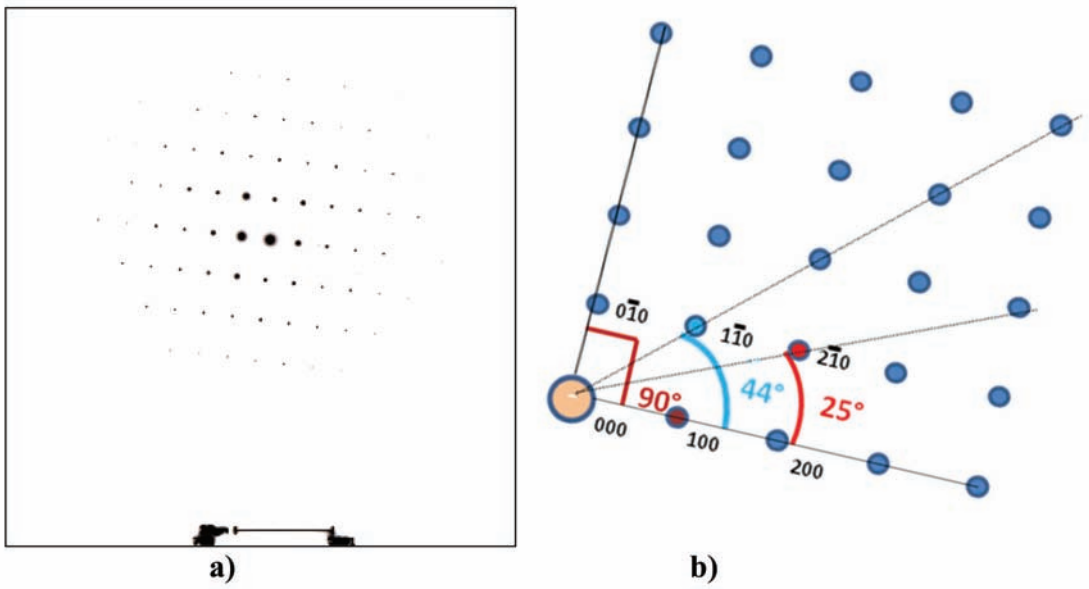

Figure 5—(a) TEM diffraction pattern for a ~Pt_3Al precipitates in a nominal Pt_{78}:Al_{11}:Ru_5:Cr_6 (at.%) alloy, (b) schematic diagram of the reciprocal lattice points system and measured angles corresponding to cubic [0 0 1] zone axis

Table IV

Summary of the best possible fit of lattice points and comparison of calculated and measured results for cubic Pt_3Al for Figure 5 (b)

			Spacing			Angles			
Lattice point			Measured	Calculated	Error	Interplanar	Measured	Calculated	Error
h	*k*	*l*	(Å)	(Å)	(%)	angles	(°)	(°)	(%)
1	0	0	4.56	4.42	3.1	-	-	-	-
0	1	0	4.79	4.42	7.7	θ_A 0 0 100	90	90	0
1	1	0	6.76	6.25	7.5	θ_B 1 0 100	44	45	2.2
2	1	0	15.69	16.55	5.2	θ_C 2 0 100	25	25	5.9

and Wenderoth *et al.*[33]. The morphology was found to be mostly cubic with a few irregular precipitates contrary to that of Hüller *et al.*[32] and Wenderoth *et al.*[33] which were mostly rounded and irregular.

Electron diffraction patterns from a number of ~Pt_3Al precipitates at different major zone axis orientations, some examples being shown here, have revealed the precipitate structure to be the high-temperature $L1_2$ cubic phase. Three zone axes only could be indexed by the cubic structure, while one, within experimental error, could be indexed by both the cubic and tetragonal structures. XRD measurements determined the lattice parameter to be a = 3.7084 Å. This compares with a = 3.876 Å at a composition of 72.8 at.% Pt determined by Bronger and Klemm[34] in 1962, and a = 3.85 – 3.91 Å for Pt_{86}:Al_{10}:X_4, where X was Ti, Cr, Ru, Ta, and Ir, by Hill *et al.*[9].

Conclusions

The analysis of the four different major zone axis diffraction patterns indicated that the cubic phase was the only fit for three of them, while for the first case it was less conclusive, leaning slightly to the tetragonal structure. Thus, the structure of ~Pt_3Al was deduced to be cubic. The proportion of the ~Pt_3Al precipitates in the (Pt) matrix is the highest recorded to date.

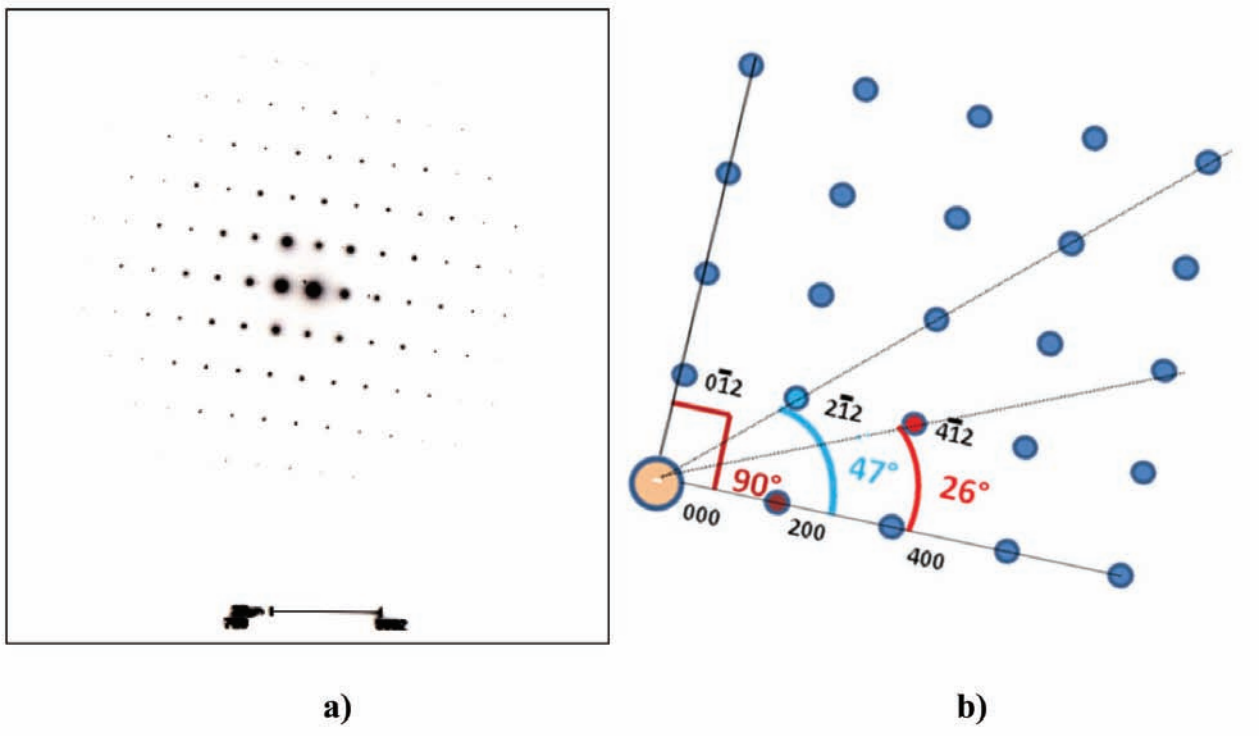

Figure 6—(a) TEM diffraction pattern for a ~Pt_3Al precipitates in a nominal Pt_{78}:Al_{11}:Ru_5:Cr_6 (at.%) alloy, (b) schematic diagram of the reciprocal lattice points system and measured angles corresponding to the cubic [0 2 1] zone axis

Table V

Summary of the best possible fit of lattice points and comparison of calculated and measured results for cubic Pt_3Al for Figure 6 (b)

			Spacing			Angles			
Lattice point			Measured	Calculated	Error	Interplanar	Measured	Calculated	Error
h	*k*	*l*	(Å)	(Å)	(%)	angles	(°)	(°)	(%)
2	0	0	8.12	8.84	8.1	-	-	-	-
0	1	2	8.93	9.89	9.7	θ_A 0 2 200	90	90	0
2	1	2	12.01	13.27	9.5	θ_B 2 2 200	47	48.19	2.5
4	1	2	19.48	20.26	3.9	θ_C 4 2 200	26	26.57	2.2

Future work

It is planned that high-temperature differential thermal analyses (DTA) will be undertaken as part of this investigation. During DTA, temperature differences between the sample and the thermally inert material are measured during heating or cooling conditions. The DTA curve records these differences during reactions in the sample, showing thermal effects as deviations from the zero line.

Hardness measurements of the samples will also be undertaken. Photographs of the hardness indentions will be taken using an optical microscope to obtain a qualitative evaluation of the alloys' toughness and where possible, slipping modes. An analysis of the hardness results, together with the TEM results, will be conducted and where possible the relationship between microstructure and mechanical properties deduced. Nanoindentation of the individual phases will be done so that the nano-hardness and modulus of elasticity of both the ~Pt_3Al precipitates and the matrix can be compared. These values will then be compared with other commercial alloys such as the single crystal Ni-base superalloys PWA 1484 and CMSX-4.

Acknowledgements

Mintek and the University of the Witwatersrand are acknowledged for availability of research resources. Financial assistance from the South African Department of Science and Technology (DST), National Research Foundation (NRF), and the Mellon Foundation is gratefully acknowledged.

References

1. Sims, C.T., Stoloff. N.S., and Hagel, W.C. Supperalloys II: High Temperature Materials for Aerospace and Industrial Power. Wiley Inter-Science, New York, 1987.
2. Yamabe-Mitarai, Y., Ro, Y., Maruko, T., Yokokawa, T., and Harada, H. PGM-based refractory superalloys for ultra-high temperature use. *Structural Intermetallics 1997. Proceedings of the 2nd International Symposium on Structural Intermetallics*, Seven Springs, Champion, USA, 21-26 Sep. 1997, Nathal, M.V., Darolia, R., Liu, C.T., Martin, P.L., Miracle, D.B., Wagner, R., and Yamaguchi M. (eds). The Minerals, Metals & Materials Society, pp. 805–814.

3. Massalski, T.B. Binary Alloy Phase Diagrams. ASM International, Ohio, 1990.

4. Mishima, Y., Oya, Y., and Suzuki, T. $L1_2 \Leftrightarrow D0'c$ martensitic transformation in Pt_3Al and Pt_3Ga. *Proceedings of the International Conference on Martensitic Transformations*. Japan Institute of Metals, 1986. pp. 1009–1014.

5. Douglas, A., Neethling, J.H., Santamarta, R., Schryvers, D., and Cornish, L.A. Unexpected ordering behaviour of Pt3Al intermetallic precipitates. *Journal of Alloys and Compounds*, vol. 432, 2007. pp. 96–102.

6. Wolff, I.M. and Hill, P.J. Platinum metals-based intermetallics for high-temperature service. *Platinum Metals. Review*, vol. 44, no. 4, 2000. pp. 158–166.

7. Hill, P.J., Adams, N., Biggs, T., Ellis, P., Taylor, S. and Wolff, I.M. Platinum alloys based on Pt-Pt_3Al for ultra-high temperature use. *Materials. Science and Engineering*, vol. A338, 2002. pp. 133–141.

8. Hill, P.J., Biggs, T., Ellis, P., Hohls, J., Taylor S., and Wolff, I.M. An assessment of ternary precipitation-strengthened Pt alloys for ultra-high temperature applications. *Materials Science and Engineering*, vol. A301, 2001. pp. 167-179.

9. Hill, P.J., Yamabe-Mitarai, Y., Murakami, H., Cornish, L.A., Witcomb, M.J., Wolff, I.M., and Harada, H. The precipitate morphology and lattice mismatch of ternary (Pt)/Pt_3Al alloys. *3rd International. Symposium On Structural Intermetallics*, Snow King Resort, Jackson Hole, Wyoming, USA, 23–27 September 2001.Demker, K.J., Dimiduk, D.M., Clemens, H., Darobia, R., Inui, H., Larsen, J.M., Sukka, V.K., Thomas, M., and Whitten Berger, J.D. (eds). Warregdale, The Minerals, Metals & Materials Society), 2001. pp. 527–533.

10. Biggs, T. An Investigation into Displacive Transformations in Platinum Alloys. PhD thesis, University of the Witwatersrand 2001.

11. Biggs, T., Hill, P.J., Cornish, L.A., and Witcomb, M.J. An investigation of the Pt-Al-Ru diagram to facilitate alloy development. *Journal of Phase Equilibria*, vol. 22, no. 3, 2001. pp. 214–218.

12. Hill, P.J. Cornish, L.A., Ellis, P., and Witcomb, M.J. The effect of Ti and Cr additions on the phase equilibria and properties of (Pt)/Pt_3Al alloys. *Journal of Alloys and Compounds*, vol. 322, 2001. pp. 166–175.

13. Cornish, L. A., Süss, R., Douglas, A., Chown, L. H., and Glaner, L. The Platinum Development Initiative: platinum-based alloys for high temperature and special applications: part I. *Platinum Metals Review*, vol. 53, no. 1, 2009. pp. 2–10.

14. Cornish, L.A., Fischer, B., and Voelkl, R. Development of platinum group metal based superalloys for high temperature use. *Materials Research Bulletin*, vol. 28, no. 9, 2003. pp. 632–638.

15. Cornish, L.A., Süss, R., Chown, L.H., and Glaner, L. The Platinum Development Initiative: platinum-based alloys for high temperature and special applications: part III. *Platinum. Metals. Review*, vol. 53, no. 3, 2009. pp. 155–163.

16. Douglas, A., Hill, P.J., Cornish, L.A., and Süss, R. The Platinum Development Initiative: platinum-based alloys for high temperature and special applications: part II *Platinum. Metals Review*, vol. 53, no. 2, 2009. pp. 69–77.

17. Cornish, L.A., Süss, R., Chown, L.H., and Glaner, L. The Platinum Development Initiative: platinum-based alloys for high temperature and special applications: part III. *Platinum Metals Review,* vol. 53, no. 3, 2009. pp. 155–163.

18. Shongwe, M.B. Optimisation of Compositions and Heat Treatments of Pt-Based Superalloys. M.Sc. Dissertation, University of the Witwatersrand, 2009.

19. Shongwe, M.B., Cornish, L.A., and Süss, R. Improvement of ~Pt_3Al volume fraction and hardness in a Pt-Al-Ru-Cr Pt-based superalloy. *Advanced Metals Initiative Conferenc*e, Gold Reef City, Johannesburg, 18–19 November 2008 [on CD].

20. Shongwe, M.B., Odera, B., Samal, S., Ukpong, A.M., Watson, A., Süss, R., Chown, L.H., Rading, G.O., and Cornish, L.A. *Light Metals Conference, Assessment of Microstructures in the Development of Pt-based Superalloys*, Misty Hills, Muldersdrift, South Africa, 27–29 October 2010. Johannesburg, The Southern African Institute of Mining and Metallurgy, 2010.

21. Ndlovu, G.F., Cornish, L.A., Douglas, A., Julies, B.A., and Joja, B. Characterisation of Pt-Rich alloys in the Pt-Al-Nb system. *Proceedings of the Microscopy Society of Southern Africa*, vol. 36, 2006. p. 11.

22. Ndlovu, G.F. Microstructural Investigation of the Pt-Al-Nb System. M.Sc. dissertation, University of the Western Cape, April 2007.

23. Mulaudzi, F.M.L., Cornish, L.A., and Witcomb, M.J. An SEM study of the Pt-Cr-Nb system. *Proceedings of the Microscopy Society of Southern Africa*, vol. 38, 2008. p. 24.

24. Mulaudzi, F.M.L. Constitution of the Pt-Cr-Nb System. M.Sc. dissertation, University of the Witwatersrand, 2009.

25. Samal, S., Mulaudzi, F.M.L. and Cornish, L.A. Further investigation on Pt-Cr-Nb system around the Pt_{40}:Cr_{20}:Nb_{40} composition. *Proceedings of the Microscopy Society of Southern Africa*, vol. 39, 2009. p. 58.

26. Odera, B.O., Cornish, L.A., Süss, R., and Rading, G.O. A study of phases in selected alloys from the Pt-Al-V system in the Pt-rich corner. *Proceedings of the Microscopy Society of Southern Africa*, vol. 39, 2009. p. 61.

27. Witcomb, M.J. Preparation of Pt and Pt-C foils for conventional and atomic resolution TEM. *Proceedings of the Electron Microscopy Society of South Africa*, vol. 22, 1992. pp. 39–40.

28. Murr, L.E. Electron Optical Applications in Materials Science. McGraw-Hill, New York, 1970.

29. Loretto, M.H. and Smallman, R.E. Defect Analysis in Electron Microscopy. T. & A. Constable, Edinburgh, 1975.

30. Huch, R. and Klemm, W. *Zeitschrift Anorganische Chemie*, vol. 329, 1964. pp. 123–135.

31. Biggs, T., Cortie, M.B., Witcomb, M.J., and Cornish, L.A. Platinum alloys for shape memory applications. *Platinum. Metals Review*, vol. 47, no. 4, 2003. pp. 142–156.

32. Hüller, M., Wenderoth, M., Vorberg, S., Fischer, B., Glatzel, U., and Völkl, R. Optimization of composition and heat treatment of age-hardened Pt-Al-Cr-Ni alloys. *Metallurgical and Matererials Transactions A*, vol. 36A, no. 3A, 2005. pp. 681–689.

33. Wenderoth, M., Cornish, L.A., Süss, R., Vorberg, S., Fischer, B., and Glatzel, U. On the development and investigation of quaternary Pt-based superalloys with Ni additions. *Metallurgical and Materials Transactions A*, vol. 36 A, 2005. pp. 567–575.

34. Bronger, W. and Klemm, W. *Zeitschrift Anorganische Chemie*, vol. 319, 1962. pp. 58–81. ◆